Curvelet sparse regularization for differential phase-contrast X-ray imaging

Matthias Wieczorek*, Jürgen Frikel†, Jakob Vogel*, Franz Pfeiffer‡, Laurent Demaret†, and Tobias Lasser*†

* Chair for Computer Aided Medical Procedures (CAMP), Technische Universität München, Germany
wieczore@cs.tum.edu

†Institute of Biomathematics and Biometry, Helmholtz Zentrum München, Germany

‡ Chair of Biomedical Physics, Technische Universität München, Germany

Abstract—Differential phase contrast imaging (DPCI) enables the visualization of soft tissue contrast using X-rays. In this work we introduce a reconstruction framework based on curvelet expansion and sparse regularization for DPCI. We will show that curvelets provide a suitable data representation for DPCI reconstruction that allows preservation of edges as well as an exact analytic representation of the system matrix. As a first evaluation, we show results using simulated phantom data.

I. Introduction

One of the main shortcomings of conventional x-ray computed tomography (CT) is the low contrast within the soft tissue regions. Differential phase-contrast imaging (DPCI) is an emerging imaging modality which was developed to address this issue. It was shown in [1], that this technique improves the visualization of soft tissues upon conventional X-ray computed tomography (CT).

The basic idea of DPCI consists in performing phase-sensitive x-ray measurements (rather than imaging the absorption coefficient) and the reconstruction of the refraction coefficient $f : \mathbb{R}^2 \to \mathbb{R}$. The mathematical model describes the relationship between the phase change and the refraction coefficient f in the following way, cf. [1], [2], [3],

$$Pf(\theta, s) = \frac{\partial}{\partial s} \int_{L(\theta,s)} f(x)\, dx, \tag{1}$$

where $L(\theta, s) = \{x \in \mathbb{R}^2 : x_1 \cos\theta + x_2 \sin\theta = s\}$ denotes a line with the normal direction $(\cos\theta, \sin\theta)^T$ and the signed distance from the origin $s \in \mathbb{R}$. Given the measurements $y = Pf$, the reconstruction problem amounts to finding the refraction coefficient f from the phase shift data Pf. In this work, we consider the following noisy reconstruction problem

$$y^\delta = Pf + \eta, \tag{2}$$

where η is the noise component with a noise level $\delta > 0$, i.e., $\|\eta\|_2 \leq \delta$. To this end, we first note that the DPCI model (1) is essentially given by the first derivative of the classical Radon transform

$$Rf(\theta, s) = \int_{L(\theta,s)} f(x)\, dx, \tag{3}$$

such that $Pf(\theta, s) = \frac{\partial}{\partial s} Rf(\theta, s)$. Therefore, techniques which were originally developed for conventional CT can be transferred to DPCI. For example, in [4], the well-known filtered backprojection (FBP) algorithms has been adapted for reconstruction from DPCI data. However, in order to achieve an adequate reconstruction quality, FBP needs a large number of projections. In addition to that, it is well-known that FBP performs poorly in the presence of noise.

To address these issues, we propose a reconstruction method that is based on a series expansion framework (often called algebraic or iterative reconstruction). In this framework, the unknown function f is expanded with respect to a given dictionary $(\psi_n)_{n=1}^N$ via $f = \sum_{n=1}^N c_n \psi_n$. Then, the expansion coefficients $(c_n)_{n=1}^N$ are determined from the measurements

$$y_m = Pf(\theta_m, s_m) = \sum_{n=1}^N c_n P\psi_n(\theta_m, s_m). \tag{4}$$

by solving the linear system of equations

$$y = Pc, \tag{5}$$

where $y = (y_1, \ldots, y_M)^T$ and $P = (P_{m,n})$ is the $M \times N$ system matrix with entries $P_{m,n} = P\psi_n(\theta_m, s_m)$.

Several choices of dictionaries have been proposed for reconstruction in DPCI. For example, in [5], Köhler et al. considered a series expansions based on Kaiser-Bessel functions (also known as isotropic blob functions). Another example is the B-Spline series expansion which was investigated by Nilchian et al. in [6].

In this work, we propose an approach that is based on the expansion of f with respect to the curvelet frame, [7]. An advantage of using curvelets over other dictionaries lies in the fact that curvelet expansions allow for an edge-preserving reconstruction. In addition to that, curvelets admit an analytic representation of the system matrix.

The paper is organized as follows: in Section II we recall the definition of curvelets and recall some of their basic properties. In Section III we describe our curvelet-based discretization used for the explicit computation of the system matrix P as well as the resulting reconstruction method. Finally, in Section

IV, we illustrate our method by reconstructions of simulated phantom data.

II. Curvelets

The curvelet dictionary is a family of functions $\psi_{j,l,k} : R^2 \to C$ which has a multi-scale structure and whose main advantage is the high directionality of its fine scale atoms [7]. The construction of curvelets is done in the Fourier domain. We will make use of the following definition of the Fourier transform

$$\hat{f}(\xi) = \frac{1}{2\pi} \int_{R^2} f(x) e^{-ix\xi}\, dx.$$

We first define the generating curvelets $\psi_{j,0,0}$ at scale 2^{-j}, $j \in N_0$, by using polar coordinates $\xi = re^{i\theta}$ in the Fourier domain:

$$\hat{\psi}_{j,0,0}(re^{i\theta}) = 2^{-3j/4} \cdot W(2^{-j} \cdot r) \cdot V\left(\frac{2^{\lfloor j/2 \rfloor + 1}}{\pi} \cdot \theta\right), \quad (6)$$

where W is a radial window and V is an angular window, respectively. We require the windows W, V to be real and smooth ($W, V \in C^\infty$) such that $\operatorname{supp} W \subset (1/2, 2)$, $\operatorname{supp} V \subset (-1, 1)$. Moreover, V and W have to satisfy proper admissibility conditions, cf. [7]. The family of curvelets $\{\psi_{j,l,k}\}_{j,l,k}$ is constructed by translation and rotation of the generating curvelets $\psi_{j,0,0}$. That is, at scale 2^{-j}, the curvelet $\psi_{j,l,k}$ is defined via

$$\psi_{j,l,k}(x) = \psi_{j,0,0}(R_{\theta_{j,l}}(x - b_k^{j,l})), \quad \text{for } x \in R^2. \quad (7)$$

Here $R_{\theta_{j,l}}$ denotes the rotation matrix

$$R_{\theta_{j,l}} = \begin{pmatrix} \cos\theta_{j,l} & -\sin\theta_{j,l} \\ \sin\theta_{j,l} & \cos\theta_{j,l} \end{pmatrix}$$

with respect to the scale-dependent rotation angles $\theta_{j,l}$ and the scale-dependent locations $b_k^{j,l}$ which are defined by

$$\theta_{j,l} = l \cdot \pi \cdot 2^{-\lfloor j/2 \rfloor - 1}, \quad -2^{\lfloor j/2 \rfloor + 1} \le l < 2^{\lfloor j/2 \rfloor + 1}, \quad (8)$$

$$b_k^{j,l} = R_{\theta_{j,l}}^{-1} \left(\frac{k_1}{2^j}, \frac{k_2}{2^{j/2}}\right), \quad k = (k_1, k_2) \in Z^2. \quad (9)$$

Clearly, each curvelet is supported on a polar wedge in the Fourier domain which has a positive distance to the origin. We complete the curvelet system with the generating low-pass function $\psi_{-1,0,0}$, defined in the Fourier domain by

$$\hat{\psi}_{-1,0,0}(re^{i\theta}) = W_0(r), \quad W_0^2(r) := 1 - \sum_{j=0}^{\infty} W^2(2^{-j} r),$$

with all of its translates $\{\psi_{-1,0,k}\}_{k \in Z^2}$. The index set of the completed curvelet dictionary is now given by

$$I = \{(-1, 0, k) : k \in Z^2\} \cup \{(j, l, k) : j \in N_0, k \in Z^2, -2^{\lfloor j/2 \rfloor + 1} \le l < 2^{\lfloor j/2 \rfloor + 1}\}$$

One of the fundamental properties of the curvelet dictionary is that it constitutes a normalized tight frame for $L^2(R^2)$, cf. [7]. In particular, each $f \in L^2(R^2)$ can be expanded in terms of curvelets via

$$f = \sum_{(j,l,k) \in I} \langle \psi_{j,l,k}, f \rangle \psi_{j,l,k}. \quad (10)$$

Note that the representation (10) is directional. Indeed, in addition to the scale-parameter j and the location parameter $k = (k_1, k_2)$, the orientation parameter l corresponds to directional features of f.

III. Curvelet series expansion for DPCI

We now use curvelets in order to discretize the DPCI operator P which is defined in (1). To this end, we model f as a finite linear combination of curvelets via

$$f = \sum_{n=1}^{N} c_n \psi_n, \quad (11)$$

where $n = n(j, l, k)$ is an enumeration of the curvelet index set I and $N = |I|$. In the following, we also assume that a finite number of measurements is available, $y_m = Pf(\theta_m, s_m)$, $1 \le m \le M \in N$. Using (11), each measurement y_m can be expressed as

$$y_m = Pf(\theta_m, s_m) = \sum_{n=1}^{N} c_n P\psi_n(\theta_m, s_m). \quad (12)$$

The discrete (noise free) reconstruction problem then reads

$$y = Pc, \quad (13)$$

where P is the system matrix which is defined by

$$P_{m,n} = P\psi_n(\theta_m, s_m), \quad 1 \le m \le M, \; n \in I. \quad (14)$$

An advantage of using curvelets for the discretization lies in the fact that the Radon transform of curvelet elements can be computed analytically. In analogy to [8], we have the following result.

Theorem III.1. Let $\psi_{j,l,k}$ be a curvelet (cf. (7)) and denote $e(\theta) = (\cos\theta, \sin\theta)$. Then,

$$P\psi_{j,l,k}(\theta, s) = 2^{5j/4} V^*\left(\frac{2^{\lfloor j/2 \rfloor + 1}}{\pi}(\theta - \theta_{j,l})\right) \sqrt{2\pi} \cdot i^n W^*(2^j) \exp\left(-i\langle b_k^{j,l}, e(\theta - \theta_{j,l})\rangle - s\right)$$

where $b_k^{j,l}$ and $\theta_{j,l}$ are defined in (8) and (9). Further, $W^*(r) = rW(r)$ with the radial window function W as given above and $V^*(\alpha) = V(\alpha) + V(\alpha - \operatorname{sgn}(\alpha)\pi)$ with V denoting the angular window function.

We now consider the discrete noisy reconstruction problem

$$y^\delta = Pc + \eta, \quad (15)$$

where $\eta \in R^N$ denotes the noise component. In order to minimize the influence of noise to the reconstruction, we use variational regularization which amounts to the minimization of an energy functional of the form

$$\|Pc - y\|_2^2 + \alpha\Lambda(c), \quad (16)$$

where the first term controls the data error and the second term $\Lambda : R^N \to [0, \infty)$ is a penalty function which encodes the a-priori information about the unknown object f.

Our goal is to design an edge-preserving reconstruction method based on curvelet coefficients. For this purpose, we take advantage of the ability of curvelets to provide optimally sparse representation of functions with sharp edges, cf. [9]. In order to obtain a sparse vector of curvelet coefficients through minimization of (16), we use the paradigm of sparse regularization, cf.[10]. In this context, it is well-known that the ℓ^1-norm favors sparse solutions. Therefore, we solve the problem (15) by minimizing the ℓ^1-penalized functional

$$\hat{c} = \arg\min_{c \in C^N} \left(\frac{1}{2} \| Pc - y^\delta \|_2^2 + \| c \|_{1,w} \right), \qquad (17)$$

where $\| c \|_{1,w} = \sum_k w_k |c_k|$ denotes the weighted 1-norm with a weight sequence w satisfying $w_k \geq w_0 > 0$. Having computed $\hat{c}$, a solution for the original problem (2) is then given by applying the synthesis operator to the regularized curvelet coefficients $\hat{c}$, i.e.,

$$f^* = \sum_{n=1}^{N} \hat{c}_n \psi_n. \qquad (18)$$

The computation of a reconstruction by (17), (18) is stable and edge-preserving.

IV. Results

A. Implementation

Our implementation of the curvelet transform is written in C++ and is based on polar coordinates in the Fourier domain. Note that the CurveLab toolbox [11] uses a slightly different approach with coronization based on concentric squares instead of concentric circles.

For sparse regularization, one of the most effective methods is the iterative soft-thresholding algorithm (ISTA) as suggested in [10]. We implemented the fast iterative soft-thresholding algorithm (FISTA) variant as proposed in [12]. In both algorithms every minimizer c^* of the ℓ^1-penalized reconstruction problem is a fixed point of the following iteration:

$$c^*_{k+1} = S_{\lambda w}\left(c^*_k - \lambda P^*(Pc^*_k - y^\delta) \right).$$

Here, S_τ denotes the soft-thresholding operator of x with threshold τ:

$$S_\tau(x) = \begin{cases} x - \mathrm{sgn}(x)\tau & |x| \geq \tau \\ 0 & \text{else.} \end{cases}$$

The step-size $\lambda > 0$ is chosen according to the Barzilai-Borwein method (cf. [13]). For our first reconstructions, we use a constant parameter $w = 0.01$. We will refer to our ℓ^1-regularized reconstruction as Curvelet Sparse Regularization (CSR), cf. (17) and (18). Additionally, we implemented the Conjugate Gradient (CG) method. We have used the CG to solve the un-regularized tomographic problem (15). In the following, we will compare the results of reconstructions obtained via FBP to those of the CG based reconstruction as well as our CSR based reconstructions. In both implementations, CSR as well as CG, we have used the closed form formula given in Theorem III.1 in order to compute the elements of the system matrix.

B. Setup and datasets

To evaluate our method, we applied the forward model to the Shepp-Logan phantom. We compare FBP (with the adjusted filter for DPCI [4]) to both of our curvelet based iterative methods - CG and CSR. Both reconstructions, CG and CSR, were produced using 200 iterations. We start our evaluation by taking 360 projections within the angular range of 0° - 180°. The results are shown in Fig. 1.

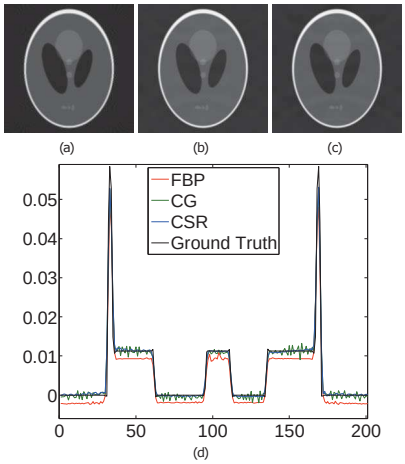

Fig. 1. (a) FBP (SNR: 12.7 dB), (b) CG (SNR: 15.7 dB), (c) CSR (SNR: 15.9 dB), (d) Line profile ($y = 100$)

The curvelet based methods provide visually promising results. Additionally, we present a line profile (see. Fig. 1 (d)) which clearly shows our curvelet based methods to be much closer to the ground truth than the FBP method. The signal to noise ratio (SNR) shows an increase from 12.7dB for FBP up to 15.9dB for CSR.

However, having a closer look we observe two additional phenomena: First, our current implementation of the curvelet based methods exhibits Gibbs-like effects. Second, we find the CG results to show high frequent noise in contrast to the FBP results. Thus, we suppose this noise is linked to the oscillating behaviour of the curvelet elements. This noise gets clearly reduced by the CSR method, while sharpness of the edges is preserved. The given line profile additionally shows, this noise reduction when using CSR in contrast to the CG method.

We continue our evaluation by reducing the number of projections taken to 60 by increasing the angular spacing from 0.5° to 3°. The corresponding results are shown in Fig. 2. The line profile in Fig. 2 (d) as well as the SNR increase from 11.1dB (FBP) to 14.3dB (CSR) emphasizes our previous results. However, in this case, we also observe Gibbs artefacts and a noise reduction when using the CSR method.

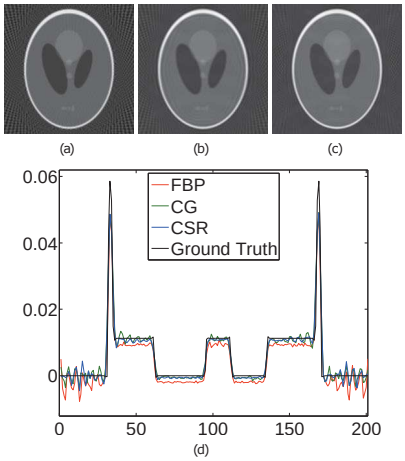

Fig. 2. (a) FBP (SNR: 11.1 dB), (b) CG (SNR: 13 dB), (c) CSR (SNR: 14.3 dB), (d) Line profile (y = 100)

V. Conclusion

In this work we have introduced a curvelet based framework for differential phase-contrast imaging. In particular, we have presented an analytically exact discretization of the DPCI operator. Moreover, we applied the curvelet sparse regularization to the reconstruction problem of DPCI. Our first reconstruction results show that the method is promising, but still requires further work to achieve better results.

We believe that the curvelet representation provides a solid basis for extending reconstruction methods towards reducing the radiation exposure by exploiting the sparsity and edge-preserving properties of curvelets.

Acknowledgment

This work was partially funded by the DFG Cluster of Excellence MAP and DFG SFB 824.

References

[1] F. Pfeiffer, T. Weitkamp, O. Bunk, and C. David, "Phase retrieval and differential phase-contrast imaging with low-brilliance X-ray sources," Nature Physics, vol. 2, no. 4, pp. 258–261, Mar. 2006.

[2] J. Kastner, B. Plank, and G. Requena, "Non-destructive characterisation of polymers and Al-alloys by polychromatic cone-beam phase contrast tomography," Materials Characterization, vol. 64, pp. 79–87, Feb. 2012.

[3] F. Pfeiffer, M. Bech, O. Bunk, P. Kraft, E. F. Eikenberry, C. Brönnimann, C. Grünzweig, and C. David, "Hard-X-ray dark-field imaging using a grating interferometer," Nature Materials, vol. 7, no. 2, pp. 134–137, Jan. 2008.

[4] F. Pfeiffer, O. Bunk, C. Kottler, and C. David, "Tomographic reconstruction of three-dimensional objects from hard X-ray differential phase contrast projection images," Nuclear Instruments and Methods in Physics Research Section A: Accelerators, Spectrometers, Detectors and Associated Equipment, vol. 580, no. 2, pp. 925–928, Oct. 2007.

[5] T. Köhler, B. Brendel, and E. Roessl, "Iterative reconstruction for differential phase contrast imaging using spherically symmetric basis functions," Medical Physics, vol. 38, no. 8, p. 4542, 2011.

[6] M. Nilchian and M. Unser, "Differential phase-contrast X-ray computed tomography: From model discretization to image reconstruction," in Biomedical Imaging (ISBI), 2012 9th IEEE International Symposium on. IEEE, 2012, pp. 90–93.

[7] E. J. Candès and D. L. Donoho, "Continuous curvelet transform. II. Discretization and Frames," Applied and Computational Harmonic Analysis, vol. 19, no. 2, pp. 198–222, 2005.

[8] J. Frikel, "Sparse regularization in limited angle tomography," Applied and Computational Harmonic Analysis, vol. 34, no. 1, pp. 117–141, 2013.

[9] E. Candès and D. Donoho, "New tight frames of curvelets and optimal representations of objects with piecewise C2 singularities," Communications on Pure and Applied Mathematics, vol. 57, no. 2, pp. 219–266, 2003.

[10] I. Daubechies, M. Defrise, and C. De Mol, "An iterative thresholding algorithm for linear inverse problems with a sparsity constraint," Communications on Pure and Applied Mathematics, vol. 57, no. 11, pp. 1413–1457, 2004.

[11] E. J. Candès, L. Demanet, D. L. Donoho, and L. Ying, "Fast Discrete Curvelet Transforms," Multiscale Modeling and Simulation, vol. 5, no. 3, pp. 861–899, 2006.

[12] A. Beck and M. Teboulle, "A Fast Iterative Shrinkage-Thresholding Algorithm for Linear Inverse Problems," SIAM Journal on Imaging Sciences, vol. 2, no. 1, Jan. 2009.

[13] J. Barzilai and J. Borwein, "Two-point step size gradient methods," IMA Journal of Numerical Analysis, vol. 8, no. 1, pp. 141–148, 1988.